Macromolecules

Article

pubs.acs.org/Macromolecules

Formation of Helical Phases in Achiral Block Copolymers by Simple Addition of Small Chiral Additives

Li Yao,[†] Xuemin Lu,[†,‡] Shuangshuang Chen,[‡] and James J. Watkins*[,†]

[†]Department of Polymer Science and Engineering, University of Massachusetts Amherst, 120 Governors Drive, Amherst, Massachusetts 01003, United States

[‡]School of Chemistry and Chemical Engineering, Shanghai Jiao Tong University, 800 Dongchuan Rd., Shanghai 200240, P. R. China

Supporting Information

ABSTRACT: Helical superstructures were induced in poly(ethylene oxide)-*b*-poly(*tert*-butyl acrylate) (PEO-*b*-PtBA) achiral diblock copolymers (BCPs) through the simple addition of pure enantiomers of tartaric acid. Hydrogen bond interactions between tartaric acid and poly(ethylene oxide) (PEO) block not only enhance the phase segregation strength of the PEO-based block copolymer but also transfer the chiral information from the additive into the achiral backbone to induce the conformational chirality. The helical phase was formed after thermal annealing with a pitch of ∼25 nm and confirmed by transmission electron microscopy (TEM) and TEM tomography. The handedness of helices can be easily selected by choice of the corresponding enantioisomer of tartaric acid.

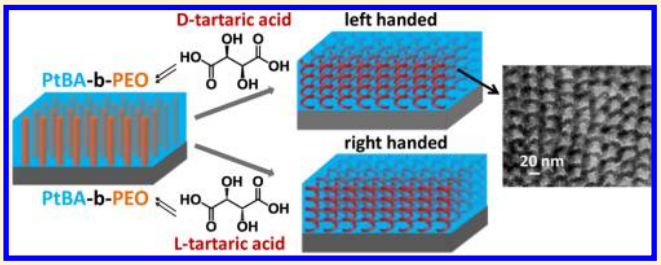

INTRODUCTION

Ordered nanostructures can be achieved by the self-assembly of various molecular units, including nanoparticles,[1−6] nanowires,[7−12] nanorods,[13−16] nanotubes,[17−24] colloids,[25−27] and block copolymers,[28−37] through noncovalent interactions. Among these, block copolymers have been studied thoroughly in recent years due to facile accessibility of regular periodic structures of controlled size and morphology.[38−48] Typically spherical, cylindrical, lamellar, and gyroid morphologies are obtained by controlling the number of repeat units (N), segregation strength (χ), block volume fraction (f), and even polydispersity index (PDI) of the block copolymers.[49−51] However, numerous structures of interest including biological inspired morphologies such as helices are not easily generated in typical block copolymer systems.

Helical superstructures are relevant to a number of life science and physical applications including metamaterials.[52,53] The formation of helical structures of different length scales[54] has been realized in solution using synthetic supramolecular chiral molecules and assemblies,[55−60] resulting in helical chain conformations[61−66] and helical aggregations.[67−71] However, it remains a challenge to achieve well-ordered 3-D arrays of nanohelices in solid or melt systems. Previously, the Ho group[72,73] used a chiral diblock copolymer system, poly(styrene)-*b*-poly(L-lactide) (PS-*b*-PLLA), to achieve nanohelical superstructures. In these materials, the chiral nature of the repeat units in the PLLA block is the driving force for the final structure. The requirement for chirality within the block copolymer backbone complicates the BCP synthesis and limits the versatility of functional blocks. The Jinnai group recently used an achiral triblock terpolymer, polystyrene-*b*-polybutadiene-*b*-poly(methyl methacrylate) (SBM),[74] to achieve a helical morphology in the bulk. However, interactions of each selected blocks are very specific, and the molecular weight range of each block required to achieve assembly is very narrow. Moreover, there is no control of the handedness of the helices in this system.

In this report we describe the straightforward use of additive driven self-assembly to achieve helical phases in an achiral block copolymer system. Additive driven self-assembly has been previously investigated in our group as a method to enhance block copolymer phase separation and achieve high additive concentrations in well-ordered systems. This method is based on the selective interaction between one segment of the block copolymer and the additives, including homopolymers,[75,76] small functional molecules,[77,78] and nanoparticles[79−81] to increase the segregation strength of the system and to generate ordered nanostructures for a variety of applications. In this report tartaric acid is selected as a chiral additive to a PEO-based achiral diblock copolymer, poly(ethylene oxide)-*b*-poly(*tert*-butyl acrylate) (PEO-*b*-PtBA).[82] The chiral information from the additive is transferred to the achiral block copolymer morphology to yield well-ordered helical structures, and at the same time the additive increases the segregation strength of the system.

Received: August 20, 2014
Revised: September 25, 2014
Published: October 3, 2014

   dx.doi.org/10.1021/ma501714g | *Macromolecules* 2014, 47, 6547−6553

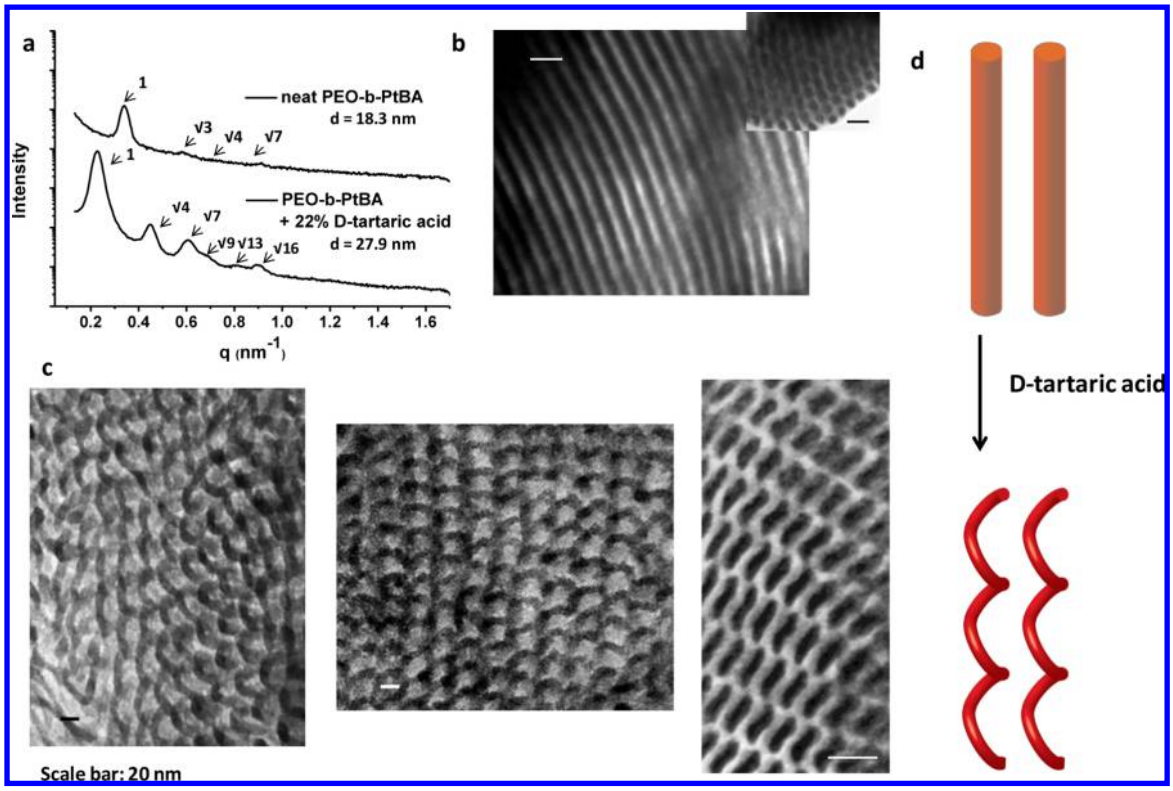

Figure 1. SAXS integration (a) of neat PEO-*b*-PtBA (18K, 72.3 wt % PtBA, PDI = 1.12) and PEO-*b*-PtBA (18K, 72.3 wt % PtBA, PDI = 1.12) blended with 22 wt % D-tartaric acid drop-cast from DMF. (b) TEM characterization of neat PEO-*b*-PtBA (18K, 72.3 wt % PtBA, PDI = 1.12) after cryo-microtoming and RuO_4 staining. (c) TEM characterization of PEO-*b*-PtBA (18K, 72.3 wt % PtBA, PDI = 1.12) blended with 22 wt % D-tartaric acid after cryo-microtoming and RuO_4 staining. All samples were annealed at 90 °C for 36 h before tests, and all SAXS data were taken at 90 °C above the melting point of PEO. (d) Schematic demonstration of the left-handed helices developed from cylinders by blending with D-tartaric acid.

EXPERIMENTAL SECTION

Materials. 2-Bromo-2-methylpropionyl bromide was bought from Sigma-Aldrich. *tert*-Butyl acrylate, copper(I) bromide (CuBr), copper-(II) bromide, anisole, and *N*,*N*,*N*′,*N*′,*N*″-pentamethyldiethylenetriamine (PMDETA) were from Acros Organics. Poly(ethylene glycol) methyl ether (5K, PDI = 1.06) was from Polymer Source. Ruthenium tetroxide, 0.5% stabilized aqueous solution was from Electron Microscopy Sciences.

Block Copolymer Synthesis. PEO end-group functionalization and PEO-*b*-PtBA block copolymer synthesis were performed following the same procedure as we used in previous work.[82] Atom transfer radical polymerization (ATRP) was used for the PEO-*b*-PtBA synthesis based on the established procedure.[83]

Polymer Characterization. The synthesized block copolymers were characterized by gel permeation chromatography (GPC) and ^{1}H NMR spectroscopy. The detailed conditions for GPC and 1H NMR were the same as our previous work.[82]

Small-Angle X-ray Scattering (SAXS). PEO-*b*-PtBA was blended with tartaric acid at a given mass ratio in DMF or anhydrous ethanol and then drop-cast on glass slides dried at room temperature for DMF and baked at 60 °C for ethanol. Thermal annealing at 90 °C under vacuum for 36 h was then applied to those samples. After being scraped from the glass slides, those dried bulk samples were then placed in the center of metal washers, sandwiched by Kapton film, and placed on a vertical holder with a temperature controller. The whole system of SAXS was under vacuum during measurement, and the samples were equilibrated at 90 °C for 20 min before measurement. The detailed condition for SAXS was the same as our previous work.[82]

Transmission Electron Microscopy (TEM). A JEOL 2000FX electron microscope was used for TEM measurement which operated at an accelerating voltage of 200 kV. A Leica Ultracut microtome was used to directly cut the bulk sample using a diamond knife conducted at a low-temperature environment of −120 °C and with the diamond knife at temperature of −110 °C. The thin pieces of the samples were then detached from the diamond knife and transferred to copper grids with carbon films. The copper grids with the sample pieces were then stained with ruthenium tetraoxide (0.5% stabilized aqueous solution) for about 10 min before TEM measurement.

TEM Tomography. The electron tomography was measured on a Tecnai F20 FEG transmission electron microscope (FEI, The Netherlands) operated at 200 kV. The sample grids were placed in a Fischione 2020 single-tilt holder (Export, PA). The single-tilt series were collected at the increment of 1° over a ±60° range using a FEI Eagle 4K × 4K CCD camera and imaging software Explore3D. Images were aligned using gold particles, and the final tomograms were reconstructed using the *R*-weighted algorithm of the IMOD software.

Circular Dichroism. The CD spectra were acquired on a circular dichroism spectrometer (JASCO J-815, Japan). The solution samples of PEO-*b*-PtBA (18K, 72.3 wt % PtBA, PDI = 1.12), PEO-*b*-PtBA blended with D-tartaric acid, and PEO-*b*-PtBA blended with L-tartaric acid were prepared in THF with the concentration of about 10 mg/mL. The path length of the quartz cuvettes was 1.0 mm. The bulk film of PEO-*b*-PtBA blended with D- or L-tartaric acid was prepared by drop-casting the THF solution on a quartz slides, which were then dried at room temperate followed by thermal annealing 90 °C for 36 h. And the samples were then measured directly by the CD instrument.

RESULTS AND DISCUSSION

Previously our group showed that enantiopure tartaric acid effectively enhances segregation strength and ordering through the hydrogen bonding between the acid and the PEO blocks of the weakly segregated system PEO-*b*-PtBA.[82] The interactions between the carboxylic acid of tartaric acid and the PEO block completely inhibit PEO crystallization and dramatically enhance the segregation strength of the system. This

dx.doi.org/10.1021/ma501714g | *Macromolecules* 2014, 47, 6547−6553

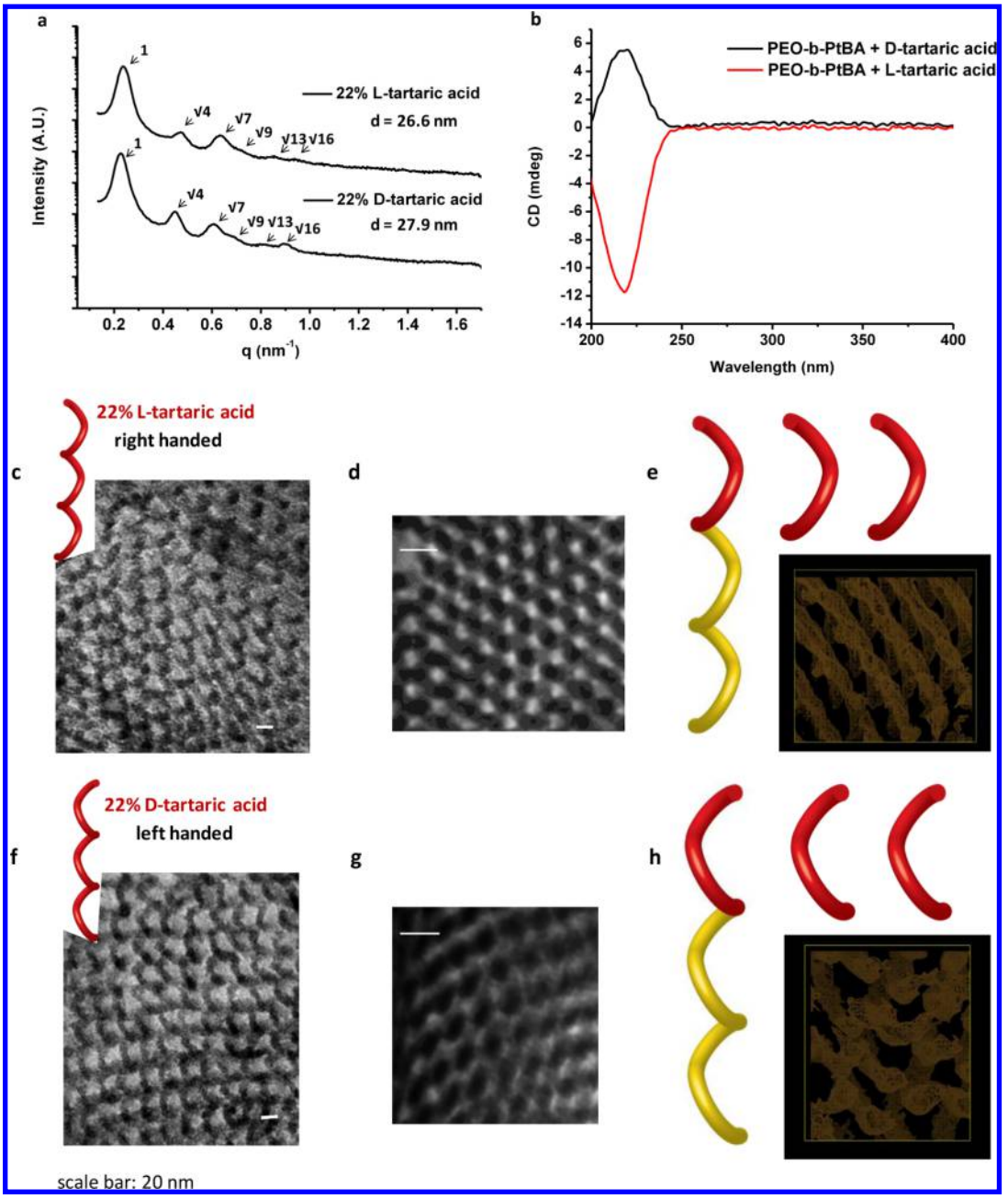

Figure 2. (a) SAXS integrations of PEO-*b*-PtBA (18K, 72.3 wt % PtBA, PDI = 1.12) blended with 22 wt % L-tartaric acid and with 22 wt % D-tartaric acid drop-cast from DMF. (b) CD spectra of bulk films made of PEO-*b*-PtBA blended with 22 wt % D-tartaric acid and PEO-*b*-PtBA blended with 22 wt % L-tartaric acid. (c, d, f, g) TEM characterization of PEO-*b*-PtBA (18K, 72.3 wt % PtBA, PDI = 1.12) blended with 22 wt % L-tartaric acid with projection perpendicular to the helix axis (c) and parallel to the axis (d) and PEO-*b*-PtBA (18K, 72.3 wt % PtBA, PDI = 1.12) blended with 22 wt % D-tartaric acid with projection perpendicular to the helix axis (f) and parallel to the axis (g) after cryo-microtoming and RuO_4 staining. (e, h) 3D tomograms for PEO-*b*-PtBA (18K, 72.3 wt % PtBA, PDI = 1.12) blended with 22 wt % L-tartaric acid (e) and 22 wt % D-tartaric acid (h) with corresponding schematic demonstration of right-handed helices for L-tartaric acid (e) and left-handed helices for D-tartaric acid (h). All samples were annealed at 90 °C for 36 h before tests, and all SAXS data were taken at 90 °C above the melting point of PEO.

additive-driven self-assembly approach can even induce order from an otherwise completely disordered system.[82]

In this study, PEO-*b*-PtBA with molecular weight of 18K, a PtBA composition of 72.3 wt %, and a PDI of 1.12 was used. The block copolymer was synthesized by end-group functionalization of PEO followed by atom transfer radical polymerization (ATRP). Bulk samples of neat PEO-*b*-PtBA and PEO-*b*-PtBA/tartaric acid composite were prepared by drop-casting on a glass slide from DMF solution (2.6 wt % of polymer) at 60 °C. After thermal annealing in a vacuum oven at 90 °C for 36 h, small-angle X-ray scattering (SAXS) was used to characterize the self-assembled nanostructures in the bulk systems. The scattering peaks in Figure 1a for neat PEO-*b*-PtBA reveal a cylindrical morphology with *d*-spacing of 18.3 nm, but the weak and poorly resolved higher order peaks also suggest weak long-range order. For the composite sample, PEO-*b*-PtBA (18K, 72.3 wt % PtBA, PDI = 1.12) blended with 22 wt % D-tartaric acid (relative to the mass of the polymer), the SAXS patterns in Figure 1a show a very sharp first-order peak accompanied by multiple higher order peaks indicating very strong segregation.

dx.doi.org/10.1021/ma501714g | *Macromolecules* 2014, 47, 6547−6553

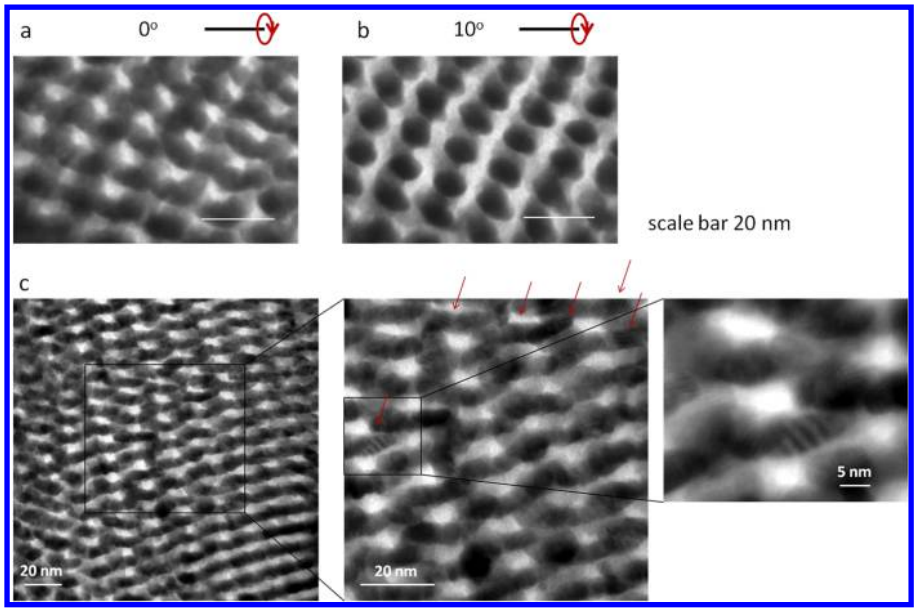

Figure 3. TEM characterization of PEO-*b*-PtBA (18K, 72.3 wt % PtBA, PDI = 1.12) blended with 22 wt % L-tartaric acid with relative sample holder tilting angle as 0° (a) and after 10° clockwise rotation (b). Substructures (c) observed in TEM of PEO-*b*-PtBA (18K, 72.3 wt % PtBA, PDI = 1.12) blended with 22 wt % L-tartaric acid.

The q value ratios of the scattering peaks are 1, $\sqrt{4}$, $\sqrt{7}$, $\sqrt{9}$, $\sqrt{13}$, and $\sqrt{16}$, which is consistent with a cylindrical morphology. Furthermore, the d-spacing is 27.9 nm, which is much larger than neat PEO-*b*-PtBA sample. In order to more clearly characterize the nanostructure of the polymer and the composite, transmission electron microscopy (TEM) was used. A cryo-microtoming (−120 °C) process was used to obtain sections with thickness of ∼50 nm. Ruthenium tetroxide (RuO_4) was used to stain the PEO domain to increase the contrast of the domains. A cylindrical morphology was clearly observed in neat PEO-*b*-PtBA sample in TEM. Figure 1b shows the TEM image in which the projection is perpendicular to the cylinder axis, with the TEM image on the upper-right corner showing the projection parallel to the cylinders axis. It is clear that the PEO (dark region) is the minor domain as shown in the parallel projection. For the composite sample, PEO-*b*-PtBA blended with 22 wt % D-tartaric acid, Figure 1c shows arrays of left-handed nanohelices with a pitch of ∼25 nm, which is consistent with the d-spacing observed in SAXS. (The handedness of the structures obtained by tartaric acid addition is confirmed by TEM tomography as discussed below.) The results suggest that chirality was successfully transferred from D-tartaric acid into the PEO-rich phase of the block copolymer/additive composite.

Previous studies[64−66,84,85] show that noncovalent bonding interactions can induce helical conformation in optically inactive achiral polymers from the chiral additives. For example, the Okamoto group[86,87] showed that chiral information can be transferred from chiral amines into achiral poly(phenylacetylene)s through an acid−base interaction to achieve helical conformation in polymer backbone. Here, the helical assemblies may result from a similar chiral induction method via hydrogen-bonding interactions between enantiopure tartaric acid and the PEO block. Thus, the chiral information on D-tartaric acid can be used to template the PEO-rich phase of the block copolymer composite, resulting in the formation of helical superstructures.

The addition of L-tartaric acid, the other enantioisomer of D-tartaric acid, was also investigated. Figure 2a shows SAXS results for PEO-*b*-PtBA (18K, 72.3 wt % PtBA, PDI = 1.12) blended with 22 wt % L-tartaric acid with the SAXS result of PEO-*b*-PtBA (18K, 72.3 wt % PtBA, PDI = 1.12) blended with 22 wt % D-tartaric acid attached to be compared. The composite yields scattering peaks that are similar to those obtained when D-tartaric acid is used as the additive and reveals a very similar d-spacing of ∼27 nm. With the addition of L-tartaric acid in PEO-*b*-PtBA, the helical superstructure was again observed in TEM as shown in Figure 2c. It is also clear that the helix in the sample loaded with L-tartaric acid is right-handed as compared with left-handed helix in the sample loaded with D-tartaric acid as shown in Figures 1c and 2f. The parallel projections of the helices with enantiopure L- and D-tartaric acid are shown in Figure 2d,g. The handedness of the helices can be selected upon loading the appropriate enantioisomer of tartaric acid, which were confirmed by TEM tomography measurements conducted at Yale School of Medicine on a Tecnai F20 FEG transmission electron microscope (FEI, The Netherlands) operated at 200 kV. The single-tilt series were collected at the increment of 1° over a ±60° range and aligned using gold particle. The final tomograms are shown in Figure 2e,h which is reconstructed using the R-weighted algorithm of the IMOD software. The right-handed helices are clearly shown in Figure 2e corresponding with PEO-*b*-PtBA blended with 22 wt % L-tartaric acid, while left-handed helices for composite blended with 22 wt % D-tartaric acid are shown in Figure 2h.

Circular dichroism (CD) spectra were used to qualitatively study the conformational chirality of the PEO-*b*-PtBA/D-tartaric acid supermolecule. The opposite Cotton effects (wavelength dependence of the optical rotary dispersion curve) represented by the CD signals in the vicinity of absorption band of carboxylate chromophore in tartaric acid were observed in the far-ultraviolet region of the CD spectra for D- and L-tartaric acid in both solution (Figure S1) and bulk system (Figure 2b), while no signal was observed for neat PEO-

dx.doi.org/10.1021/ma501714g | *Macromolecules* 2014, 47, 6547−6553

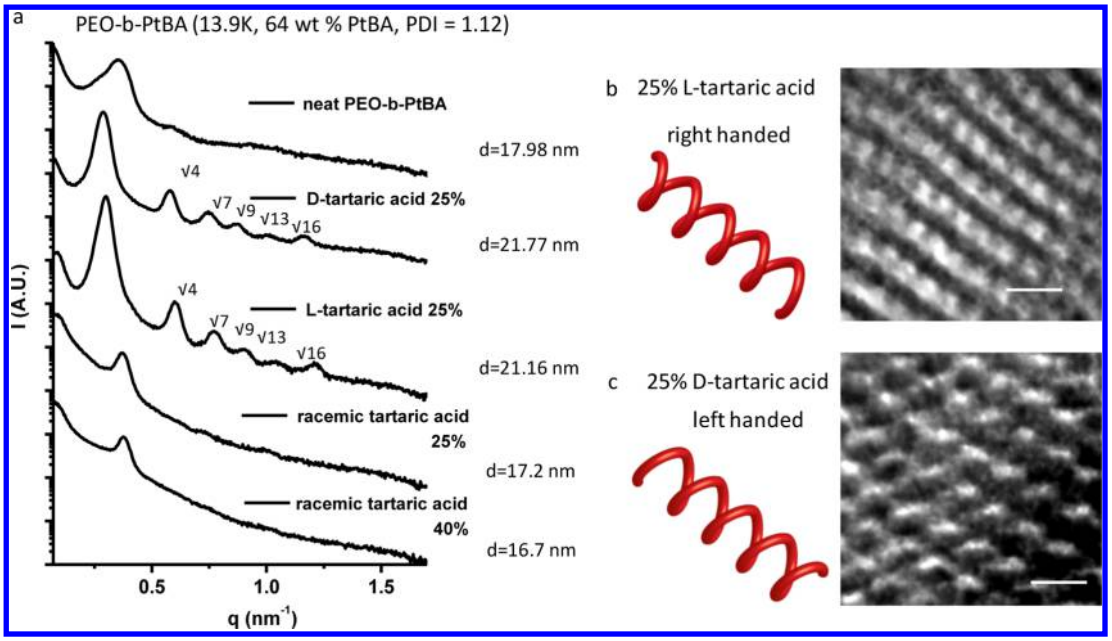

Figure 4. SAXS integrations (a) of neat PEO-*b*-PtBA (13.9K, 64 wt % PtBA, and PDI 1.12), PEO-*b*-PtBA (18K, 72.3 wt % PtBA, and PDI = 1.12) blended with 25 wt % D-tartaric acid, 25 wt % L-tartaric acid, 25 wt % racemic tartaric acid, and 40 wt % racemic tartaric acid drop-cast from ethanol. TEM characterization of PEO-*b*-PtBA (13.9K, 64 wt % PtBA, and PDI 1.12) blended with 25 wt % L-tartaric acid (b) and PEO-*b*-PtBA (13.9K, 64 wt % PtBA, and PDI 1.12) blended with 25 wt % D-tartaric acid (c) after cryo-microtoming and RuO_4 staining. All samples were annealed at 90 °C for 36 h before tests, and all SAXS data were taken at 90 °C above the melting point of PEO.

b-PtBA sample in Figure S1 (same as the background THF). Previously we used SAXS, WAXS, and AFM to confirm that no tartaric acid aggregation or macrophase separation in the supermolecule systems of PEO-*b*-PtBA/enantiopure tartaric acid occurs in the tartaric acid concentration regions of interest.[82] DSC, WAXS, and SAXS also show that D- or L-tartaric acid interacts well with PEO block to inhibit the crystallization of PEO, increase the *d*-spacing, and form the supermolecules.[82] Thus, we can exclude the possibility that the observed opposite Cotton effects of the bulk BCP films blended with D- or L-tartaric acid in Figure 4b are from the aggregation of the tartaric acid, and we can make the conclusion that the opposite conformational chirality of the supermolecule backbone actually contributes to the Cotton effects in the far-ultraviolet region of the CD spectra. Together with the TEM evidence, we confirm that the chirality is successfully transferred from the chiral additive to the backbone of the supermolecule and then to the phase of bulk system to form helical superstructures.

To better characterize the helical morphology in the PEO-*b*-PtBA/tartaric acid composite system, a rotatable sample holder was used to image the nanostructures at multiple angles. In Figure 3a,b, two TEM projection images of the same spot are shown during sample holder rotation. Figure 3a shows the micrograph of the plane projection with the direction parallel to the helix axis, while Figure 3b shows the micrograph of the plane projection with the sample holder rotated clockwise by 10°. The projection with an angle 10° away from the direction parallel to the helix axis in Figure 3b shows the helix linked with other adjacent helices, which helps to illustrate the formation of 3-D helical structures in our system. Figure 3c shows interesting substructures observed in the sample with 22 wt % L-tartaric acid loading. Parallel lines were observed with a line width smaller than 1 nm in the dark regions, the PEO domain with L-tartaric acid, as shown in Figure 3c. These substructures look very similar to DNA base pairs in the double-helix structures, which may provide information about the mechanism of the helical phase formation in our system.

In order to test the versatility of this chiral additive-driven helical superstructure formation, PEO-*b*-PtBA with different molecular weights, PEO volume fraction, and tartaric acid loadings (weight percentages in Figure 4) were used to rule out the possibility that the helical superstrucuture can only be formed in PEO-*b*-PtBA with a narrow window in the phase diagram. Thus, a PEO-*b*-PtBA with different molecular weight, PEO volume fraction, and tartaric acid loading percentage need to be used. Here, the PEO-*b*-PtBA with the molecular weight of 13.9K, the PtBA weight percentage of 64%, and PDI of 1.12 was used, which was also synthesized through PEO end-group functionalization followed by ATRP. Figure 4a shows that the neat PEO-*b*-PtBA (13.9K, 64 wt % PtBA, and PDI 1.12) is originally weakly segregated with *d*-spacing of approximately 18 nm. The addition of enantiopure tartaric acid, either L or D, again dramatically improved the ordering as shown in Figure 4a with increased *d*-spacing of 21−22 nm. The ratios of the *q* values of those scattering peaks are also 1, $\sqrt{4}$, $\sqrt{7}$, $\sqrt{9}$, $\sqrt{13}$, and $\sqrt{16}$. The interesting phenomenon is that with the addition of the racemic tartaric acid, no ordering improvement was observed even with an increased loading amount of racemic acid as shown in Figure 4. The reason is that a racemic heteropair structure formed for racemic tartaric acid with the lowest energy level identified by phase pair identity density functional theory simulations.[88] This is discussed in our previous work.[82] TEM was used to image the enantiopure tartaric acid BCP composites after staining with RuO_4. Again, right-handed helices were observed in the PEO-*b*-PtBA (13.9K, 64 wt % PtBA, and PDI 1.12) blended with L-tartaric acid and left-handed helices for D-tartaric acid.

The addition of tartaric acid to a BCP exhibiting a lamellar morphology was also investigated. PEO-*b*-PtBA with a

dx.doi.org/10.1021/ma501714g | *Macromolecules* 2014, 47, 6547−6553

molecular weight of 9.2K containing 46.6 wt % PtBA exhibits only a single peak in SAXS showing a *d*-spacing of around 13 nm. With 40 wt % L-tartaric acid loading, higher order peaks in SAXS were observed and indicate a lamellar morphology as determined by the ratios of the *q* values of those scattering peaks. To image the nanostructure, TEM was again applied after cryo-microtoming and RuO_4 staining. However, only a lamellar morphology was observed shown in Figure S2. Twisting of helices was also not observed in the PS-*b*-PDLA systems exhibiting lamellae morphology as reported by other groups.[89,90]

CONCLUSION

We describe a novel method to achieve nanohelical phases in achiral block copolymer systems by simple blending with small chiral additives. We demonstrate that a chiral block copolymer backbone is not necessary for helical phase formation. Rather, hydrogen bonding between the additives and one of the blocks can help transfer the chirality from the additives into the polymer composite through the domino effect, resulting in well-ordered nanohelical superstructures. Our methods can tolerate block copolymers with a relatively large window of molecular weight and volume ratio. We also show that no twisting was observed for composites exhibiting lamellar morphologies. This simple approach could dramatically broaden the accessibility and potential applications of the nanohelical phase.

ASSOCIATED CONTENT

Supporting Information

CD spectra of pure THF, the THF solutions of PEO-*b*-PtBA (18K, 72.3 wt % PtBA, PDI = 1.12), PEO-*b*-PtBA + 22 wt % D-tartaric acid, PEO-*b*-PtBA + 22 wt % L-tartaric acid (the concentrations of all solutions are about 10 mg/mL); SAXS integrations (a) of neat PEO-*b*-PtBA (9.2K, 46.6 wt % PtBA, and PDI 1.04), PEO-*b*-PtBA (9.2K, 46.6 wt % PtBA, and PDI 1.04) blended with 40 wt % L-tartaric acid drop-cast from ethanol; TEM characterization of PEO-*b*-PtBA (9.2K, 46.6 wt % PtBA, and PDI 1.04) blended with 25 wt % L-tartaric acid (b, c) after cryo-microtoming and RuO_4 staining (all samples were annealed at 90 °C for 36 h before tests and all SAXS data were taken at 90 °C above the melting point of PEO). This material is available free of charge via the Internet at http://pubs.acs.org.

AUTHOR INFORMATION

Corresponding Author

*E-mail: watkins@polysci.umass.edu (J.J.W.).

Notes

The authors declare no competing financial interest.

ACKNOWLEDGMENTS

This work was supported by the NSF Center for Hierarchical Manufacturing (CMMI-1025020). Facilities used in this work were supported by the Materials Research Science and Engineering Center at University of Massachusetts Amherst with the assistance from Dr. D. Thirunavukkarasu and Mr. L. Raboin. We also thank Dr. Xinran Liu from Yale School of Medicine for the electron tomography measurement. We thank Prof. S. Gido, Dr. Y. Lin, Dr. G. Lu, Dr. D. Song, T. Tsai, and Dr. W. Zhao for helpful discussions.

REFERENCES

(1) Li, M.; Schnablegger, H.; Mann, S. *Nature* **1999**, *402*, 393−395.
(2) Zeng, H.; Li, J.; Liu, J. P.; Wang, Z. L.; Sun, S. H. *Nature* **2002**, *420*, 395−398.
(3) Kotov, N. A.; Dekany, I.; Fendler, J. H. *J. Phys. Chem.* **1995**, *99*, 13065−13069.
(4) Claridge, S. A.; Mastroianni, A. J.; Au, Y. B.; Liang, H. W.; Micheel, C. M.; Frechet, J. M. J.; Alivisatos, A. P. *J. Am. Chem. Soc.* **2008**, *130*, 9598−9605.
(5) Shevchenko, E. V.; Kortright, J. B.; Talapin, D. V.; Aloni, S.; Alivisatos, A. P. *Adv. Mater.* **2007**, *19*, 4183−4188.
(6) Westcott, S. L.; Oldenburg, S. J.; Lee, T. R.; Halas, N. J. *Langmuir* **1998**, *14*, 5396−5401.
(7) Lu, W.; Lieber, C. M. *J. Phys. D: Appl. Phys.* **2006**, *39*, R387−R406.
(8) Cui, Y.; Lieber, C. M. *Science* **2001**, *291*, 851−853.
(9) Huang, Y.; Duan, X. F.; Wei, Q. Q.; Lieber, C. M. *Science* **2001**, *291*, 630−633.
(10) Javey, A.; Nam, S.; Friedman, R. S.; Yan, H.; Lieber, C. M. *Nano Lett.* **2007**, *7*, 773−777.
(11) Briseno, A. L.; Mannsfeld, S. C. B.; Reese, C.; Hancock, J. M.; Xiong, Y.; Jenekhe, S. A.; Bao, Z.; Xia, Y. N. *Nano Lett.* **2007**, *7*, 2847−2853.
(12) Briseno, A. L.; Mannsfeld, S. C. B.; Jenekhe, S. A.; Bao, Z.; Xia, Y. N. *Mater. Today* **2008**, *11*, 38−47.
(13) Rivest, J. B.; Swisher, S. L.; Fong, L. K.; Zheng, H. M.; Alivisatos, A. P. *ACS Nano* **2011**, *5*, 3811−3816.
(14) Colfen, H.; Mann, S. *Angew. Chem., Int. Ed.* **2003**, *42*, 2350−2365.
(15) Pacholski, C.; Kornowski, A.; Weller, H. *Angew. Chem., Int. Ed.* **2002**, *41*, 1188−1191.
(16) Baker, J. L.; Widmer-Cooper, A.; Toney, M. F.; Geissler, P. L.; Alivisatos, A. P. *Nano Lett.* **2010**, *10*, 195−201.
(17) Barrena, E.; Zhang, X. N.; Mbenkum, B. N.; Lohmueller, T.; Krauss, T. N.; Kelsch, M.; van Aken, P. A.; Spatz, J. P.; Dosch, H. *ChemPhysChem* **2008**, *9*, 1114−1116.
(18) Fan, S. S.; Chapline, M. G.; Franklin, N. R.; Tombler, T. W.; Cassell, A. M.; Dai, H. J. *Science* **1999**, *283*, 512−514.
(19) Dai, H. J. *Acc. Chem. Res.* **2002**, *35*, 1035−1044.
(20) Reches, M.; Gazit, E. *Science* **2003**, *300*, 625−627.
(21) Bong, D. T.; Clark, T. D.; Granja, J. R.; Ghadiri, M. R. *Angew. Chem., Int. Ed.* **2001**, *40*, 988−1011.
(22) Park, S.; Lim, J. H.; Chung, S. W.; Mirkin, C. A. *Science* **2004**, *303*, 348−351.
(23) Macak, J. M.; Tsuchiya, H.; Taveira, L.; Aldabergerova, S.; Schmuki, P. *Angew. Chem., Int. Ed.* **2005**, *44*, 7463−7465.
(24) Richard, C.; Balavoine, F.; Schultz, P.; Ebbesen, T. W.; Mioskowski, C. *Science* **2003**, *300*, 775−778.
(25) Chen, Q.; Bae, S. C.; Granick, S. *Nature* **2011**, *469*, 381−384.
(26) Yan, J.; Bloom, M.; Bae, S. C.; Luijten, E.; Granick, S. *Nature* **2012**, *491*, 578−581.
(27) Freeman, R. G.; Grabar, K. C.; Allison, K. J.; Bright, R. M.; Davis, J. A.; Guthrie, A. P.; Hommer, M. B.; Jackson, M. A.; Smith, P. C.; Walter, D. G.; Natan, M. J. *Science* **1995**, *267*, 1629−1632.
(28) Glass, R.; Möller, M.; Spatz, J. P. *Nanotechnology* **2003**, *14*, 1153−1160.
(29) Kim, S. H.; Misner, M. J.; Xu, T.; Kimura, M.; Russell, T. P. *Adv. Mater.* **2004**, *16*, 226−231.
(30) Lopes, W. A.; Jaeger, H. M. *Nature* **2001**, *414*, 735−738.
(31) Thurn-Albrecht, T.; Schotter, J.; Kästle, G. A.; Emley, N.; Shibauchi, T.; Krusin-Elbaum, L.; Guarini, K.; Black, C. T.; Tuominen, M. T.; Russell, T. P. *Science* **2000**, *290*, 2126−2129.
(32) Hamley, I. W. *Angew. Chem., Int. Ed.* **2003**, *42*, 1692−1712.
(33) Lazzari, M.; López-Quintela, M. A. *Adv. Mater.* **2003**, *15*, 1583−1594.
(34) Hawker, C. J.; Russell, T. P. *MRS Bull.* **2005**, *30*, 952−966.
(35) Park, M.; Harrison, C.; Chaikin, P. M.; Register, R. A.; Adamson, D. H. *Science* **1997**, *276*, 1401−1404.

(36) Cheng, J. Y.; Ross, C. A.; Smith, H. I.; Thomas, E. L. *Adv. Mater.* **2006**, *18*, 2505−2521.
(37) Stoykovich, M. P.; Nealey, P. F. *Mater. Today* **2006**, *9*, 20−29.
(38) Chan, V. Z.-H.; Hoffman, J.; Lee, V. Y.; Iatrou, H.; Avgeropoulos, A.; Hadjichristidis, N.; Miller, R. D.; Thomas, E. L. *Science* **1999**, *286*, 1716−1719.
(39) Hayward, R. C.; Alberius, P. C. A.; Kramer, E. J.; Chmelka, B. F. *Langmuir* **2004**, *20*, 5998−6004.
(40) Urade, V. N.; Wei, T.-C.; Tate, M. P.; Kowalski, J. D.; Hillhouse, H. W. *Chem. Mater.* **2007**, *19*, 768−777.
(41) Crossland, E. J. W.; Kamperman, M.; Nedelcu, M.; Ducati, C.; Wiesner, U.; Smilgies, D. M.; Toombes, G. E. S.; Hillmyer, M. A.; Ludwigs, S.; Steiner, U.; Snaith, H. J. *Nano Lett.* **2008**, *9*, 2807−2812.
(42) Kennemur, J. G.; Yao, L.; Bates, F. S.; Hillmyer, M. A. *Macromolecules* **2014**, *47*, 1411−1418.
(43) Bates, F. S.; Hillmyer, M. A.; Lodge, T. P.; Bates, C. M.; Delaney, K. T.; Fredrickson, G. H. *Science* **2012**, *336*, 434−440.
(44) Li, Z.; Kesselman, E.; Talmon, Y.; Hillmyer, M. A.; Lodge, T. P. *Science* **2004**, *306*, 98−101.
(45) Jang, S. G.; Audus, D. J.; Klinger, D.; Krogstad, D. V.; Kim, B. J.; Cameron, A.; Kim, S.-W.; Delaney, K. T.; Hur, S.-M.; Killops, K. L.; Fredrickson, G. H.; Kramer, E. J.; Hawker, C. J. *J. Am. Chem. Soc.* **2013**, *135*, 6649−6657.
(46) Choi, J.-H.; Ye, Y.; Elabd, Y. A.; Winey, K. I. *Macromolecules* **2013**, *46*, 5290−5300.
(47) Kelley, E. G.; Murphy, R. P.; Seppala, J. E.; Smart, T. P.; Hann, S. D.; Sullivan, M. O.; Epps, T. H. *Nat. Commun.* **2014**, *5*.
(48) Bates, C. M.; Seshimo, T.; Maher, M. J.; Durand, W. J.; Cushen, J. D.; Dean, L. M.; Blachut, G.; Ellison, C. J.; Willson, C. G. *Science* **2012**, *338*, 775−779.
(49) Bates, F. S. *Science* **1991**, *251*, 898−905.
(50) Schmitt, A. L.; Mahanthappa, M. K. *Soft Matter* **2012**, *8*, 2294−2303.
(51) Widin, J. M.; Schmitt, A. K.; Schmitt, A. L.; Im, K.; Mahanthappa, M. K. *J. Am. Chem. Soc.* **2012**, *134*, 3834−3844.
(52) Valentine, J.; Zhang, S.; Zentgraf, T.; Ulin-Avila, E.; Genov, D. A.; Bartal, G.; Zhang, X. *Nature* **2008**, *455*, 376−379.
(53) Vignolini, S.; Yufa, N. A.; Cunha, P. S.; Guldin, S.; Rushkin, I.; Stefik, M.; Hur, K.; Wiesner, U.; Baumberg, J. J.; Steiner, U. *Adv. Mater.* **2012**, *24*, OP23−OP27.
(54) Yashima, E.; Maeda, K.; Iida, H.; Furusho, Y.; Nagai, K. *Chem. Rev.* **2009**, *109*, 6102−6211.
(55) Hoshikawa, N.; Yamamoto, C.; Hotta, Y.; Okamoto, Y. *Polym. J.* **2006**, *38*, 1258−1266.
(56) Miyake, G. M.; Mariott, W. R.; Chen, E. Y. X. *J. Am. Chem. Soc.* **2007**, *129*, 6724−6725.
(57) Kamer, P. C. J.; Cleij, M. C.; Nolte, R. J. M.; Harada, T.; Hezemans, A. M. F.; Drenth, W. *J. Am. Chem. Soc.* **1988**, *110*, 1581−1587.
(58) Cornelissen, J.; Donners, J.; de Gelder, R.; Graswinckel, W. S.; Metselaar, G. A.; Rowan, A. E.; Sommerdijk, N.; Nolte, R. J. M. *Science* **2001**, *293*, 676−680.
(59) Kennemur, J. G.; Clark, J. B.; Tian, G.; Novak, B. M. *Macromolecules* **2010**, *43*, 1867−1873.
(60) Kennemur, J. G.; Novak, B. M. *Polymer* **2011**, *52*, 1693−1710.
(61) Nomura, R.; Fukushima, Y.; Nakako, H.; Masuda, T. *J. Am. Chem. Soc.* **2000**, *122*, 8830−8836.
(62) Pijper, D.; Feringa, B. L. *Soft Matter* **2008**, *4*, 1349−1372.
(63) Yashima, E.; Maeda, K.; Nishimura, T. *Chem.—Eur. J.* **2004**, *10*, 42−51.
(64) Inai, Y.; Tagawa, K.; Takasu, A.; Hirabayashi, T.; Oshikawa, T.; Yamashita, M. *J. Am. Chem. Soc.* **2000**, *122*, 11731−11732.
(65) Komori, H.; Inai, Y. *J. Phys. Chem. A* **2006**, *110*, 9099−9107.
(66) Ousaka, N.; Inai, Y. *J. Org. Chem.* **2009**, *74*, 1429−1439.
(67) Dupont, J.; Liu, G. J.; Niihara, K.; Kimoto, R.; Jinnai, H. *Angew. Chem., Int. Ed.* **2009**, *48*, 6144−6147.
(68) Cornelissen, J.; Fischer, M.; Sommerdijk, N.; Nolte, R. J. M. *Science* **1998**, *280*, 1427−1430.
(69) Malashkevich, V. N.; Kammerer, R. A.; Efimov, V. P.; Schulthess, T.; Engel, J. *Science* **1996**, *274*, 761−765.
(70) Li, C. Y.; Cheng, S. Z. D.; Ge, J. J.; Bai, F.; Zhang, J. Z.; Mann, I. K.; Chien, L. C.; Harris, F. W.; Lotz, B. *J. Am. Chem. Soc.* **2000**, *122*, 72−79.
(71) Yan, Y.; Yu, Z.; Huang, Y. W.; Yuan, W. X.; Wei, Z. X. *Adv. Mater.* **2007**, *19*, 3353−3357.
(72) Ho, R.-M.; Chiang, Y.-W.; Tsai, C.-C.; Lin, C.-C.; Ko, B.-T.; Huang, B.-H. *J. Am. Chem. Soc.* **2004**, *126*, 2704−2705.
(73) Ho, R.-M.; Li, M.-C.; Lin, S.-C.; Wang, H.-F.; Lee, Y.-D.; Hasegawa, H.; Thomas, E. L. *J. Am. Chem. Soc.* **2012**, *134*, 10974−10986.
(74) Jinnai, H.; Kaneko, T.; Matsunaga, K.; Abetz, C.; Abetz, V. *Soft Matter* **2009**, *5*, 2042−2046.
(75) Tirumala, V. R.; Daga, V.; Bosse, A. W.; Romang, A.; Ilavsky, J.; Lin, E. K.; Watkins, J. J. *Macromolecules* **2008**, *41*, 7978−7985.
(76) Tirumala, V. R.; Romang, A.; Agarwal, S.; Lin, E. K.; Watkins, J. J. *Adv. Mater.* **2008**, *20*, 1603−1608.
(77) Daga, V. K.; Anderson, E. R.; Gido, S. P.; Watkins, J. J. *Macromolecules* **2011**, *44*, 6793−6799.
(78) Daga, V. K.; Watkins, J. J. *Macromolecules* **2010**, *43*, 9990−9997.
(79) Lin, Y.; Daga, V. K.; Anderson, E. R.; Gido, S. P.; Watkins, J. J. *J. Am. Chem. Soc.* **2011**, *133*, 6513−6516.
(80) Wei, Q.; Lin, Y.; Anderson, E. R.; Briseno, A. L.; Gido, S. P.; Watkins, J. J. *ACS Nano* **2012**, *6*, 1188−1194.
(81) Yao, L.; Lin, Y.; Watkins, J. J. *Macromolecules* **2014**, *47*, 1844−1849.
(82) Yao, L.; Watkins, J. J. *ACS Nano* **2013**, *7*, 1513−1523.
(83) Davis, K. A.; Charleux, B.; Matyjaszewski, K. *J. Phys. Chem. A* **2000**, *38*, 2274−2283.
(84) Yashima, E.; Maeda, K. *Macromolecules* **2007**, *41*, 3−12.
(85) Yashima, E.; Maeda, K.; Furusho, Y. *Acc. Chem. Res.* **2008**, *41*, 1166−1180.
(86) Yashima, E.; Matsushima, T.; Okamoto, Y. *J. Am. Chem. Soc.* **1995**, *117*, 11596−11597.
(87) Kamikawa, Y.; Kato, T.; Onouchi, H.; Kashiwagi, D.; Maeda, K.; Yashima, E. *J. Phys. Chem. A* **2004**, *42*, 4580−4586.
(88) Santagata, N. M.; Lakhani, A. M.; Davis, B. F.; Luo, P.; Buongiorno Nardelli, M.; Pearl, T. P. *J. Phys. Chem. C* **2010**, *114*, 8917−8925.
(89) Zhao, W.; Liu, F.; Wei, X.; Chen, D.; Grason, G. M.; Russell, T. P. *Macromolecules* **2013**, *46*, 474−483.
(90) Zhao, W.; Chen, D.; Grason, G. M.; Russell, T. P. *Macromolecules* **2013**, *46*, 455−462.